

Universal shape characteristics for the mesoscopic polymer chain *via* dissipative particle dynamics

O. Kalyuzhnyi^{1,4}, J.M. Ilnytskyi^{1,4}, Yu.Holovatch^{1,4}

C. von Ferber^{2,3,4}

¹Institute for Condensed Matter Physics, National Acad. Sci. of Ukraine, UA-79011 Lviv, Ukraine

²Applied Mathematics Research Centre, Coventry University, Coventry, CV1 5FB, United Kingdom

³Heinrich-Heine Universität Düsseldorf, D-40225 Düsseldorf, Germany

⁴Doctoral College for the Statistical Physics of Complex Systems, Leipzig-Lorraine-Lviv-Coventry (**L**⁴), D-04009 Leipzig, Germany

Abstract. In this paper we study the shape characteristics of a polymer chain in a good solvent using a mesoscopic level of modelling. The dissipative particle dynamics simulations are performed in the $3D$ space at a range of chain lengths N . The scaling laws for the end-to-end distance and gyration radius are examined first and found to hold for $N \geq 10$ yielding reasonably accurate value for the Flory exponent ν . Within the same interval of chain lengths, the asphericity, prolateness, size ratio and other shape characteristics of the chain are found to become independent of N . Their mean values are found to agree reasonably well with the respective theoretical results and lattice Monte Carlo simulations. Broad probability distributions for the shape characteristics are found resembling in form the results of lattice Monte Carlo simulations. By means of analytic fitting of these distributions the most probable values for the shape characteristics are found to supplement their mean values.

PACS numbers: 00.00, 20.00, 42.10

Keywords: polymer, scaling, dissipative particle dynamics

1. Introduction

Universal scaling laws for the dimensional properties of flexible polymer chain in a good solvent, such as the end-to-end distance R_e and the gyration radius R_g , are well explained and understood since the groundbreaking studies by de Gennes and des Cloizeaux [1, 2]. It was found that both properties scale as

$$\langle R_e^2 \rangle \sim \langle R_g^2 \rangle \sim N^{2\nu} \quad (1)$$

for large enough numbers of monomers N , where the exponent ν is universal and depends on the dimension of space d only. Besides that, the probability distribution $p(R_e)$ is also examined in both asymptotic regimes of small and large values of R_e based on the number of chain conformations [1, 2]. Similar arguments allowed Lhuillier to suggest an heuristic form for the probability distribution $p(R_g)$ as well [3].

As far as the scaling laws are also valid for a number of other characteristics of the polymer chain, the universality and scaling properties are often treated as identical concepts. This, however, is a misconception as far as there exist characteristics that are universal but do not obey scaling laws. An example is given by the shape characteristics of polymer chains that which is in the focus of this paper. These are important in a number of applications, to mention here various catalytic activities [4, 5] and gel chromatography [6].

The fact that the shape of a polymer coil in a good solvent is not spherical is known since a classical work by Kuhn [7]. However, the understanding that certain shape properties of polymer chains are universal and depend, like scaling parameters, solely on d , is brought *via* the use of the renormalization group method (see, e.g. [8, 9]). These findings were also supported by a number of numerical simulations performed on lattice models of the self avoiding walk (SAW) [10, 11, 12, 13, 14, 15, 16, 17, 18]. One should note that the mean values for most shape characteristics are different but nonetheless close to their random walk (RW) counterparts. Some important implication here can be seen in the fact that the probability distributions for most of these characteristics are very broad and asymmetric yielding an ambiguity in the definition of their mean values. The shape of these distributions remains to be explained in a manner similar to the one given for their counterparts $p(R_e)$ [1, 2] and $p(R_g)$ [3, 19].

Most of the simulation studies mentioned above use the Monte Carlo algorithm applied to the SAW lattice model. This approach achieves very good configuration statistics by means of relatively low computation cost. Atomistic off-lattice models, on the other hand, allow one to include the effects of chain stiffness, chain composition, the role of solvent, etc. in a chemical way, but at an increased simulation time cost. A good compromise here is the use of coarse-grained approaches that combine the best of two worlds: chemical versatility and computational efficiency. One of such approaches is the dissipative particle dynamics (DPD) method [20, 21], that has already been used by a number of authors [22, 23, 24, 25, 26, 27] including two of the current authors [28], to examine the scaling properties of a polymer chain in a solvent of variable quality.

The benefit of this approach is that it provides the means to study a number of important problems related to microphase separation of amphi- and polyphilic molecules, self-assembly, adsorption, etc. (see, e.g. [29, 30, 31, 32]). Macromolecular shape plays an important role in all of the above mentioned problems. Therefore, the validation of this approach with respect to its reliability in predicting the correct macromolecular shape is of high practical interest.

This is exactly at the heart of the current study, where we apply DPD simulations to the simplest case – a single chain in a good solvent. We examine the asphericity, prolateness and a number of the other shape characteristics, as well as their probability distributions. Besides the mean values for each of these properties, we also evaluate their most probable values by means of fitting their probability distributions to respective analytic expressions. The outline of the study is as follows. The simulation approach and the properties of interest are described in Sec. 2, scaling properties and a probability distributions analysis are covered in Sec. 3, probability distributions for shape characteristics are discussed in Sec. 4 and conclusions are provided in Sec. 5.

2. Simulation approach and properties of interest

Our study is based on mesoscopic DPD simulations, which has two main advantages: (i) neglecting less important properties of a system on small length- and time-scales, and (ii) preserving hydrodynamic limits [20, 21]. A single polymer chain and an explicit solvent are contained within a cubic simulation box with a linear size of at least $5R'_g$. Here, R'_g is the estimate for the gyration radius of a chain of N monomers in a good solvent: $R'_g \approx [b(N-1)]^{0.59}$ ($b \approx 0.9$ is an estimate for an average bond length as reported in [28]). The monomers are soft beads of equal size, and each one represents either a fragment of a real polymer chain or a few molecules of a solvent. We restrict our study to the case of an athermal solvent, where all types of pairwise bead-bead interactions: polymer-polymer, solvent-solvent and polymer-solvent are identical.

The monomer coordinates \mathbf{x}_i are defined in continuous space (in contrary to most studies using the Monte Carlo method for similar studies, which, typically, are performed on a lattice). This allows to describe the phase space of conformations by chains of shorter length. On the other hand, the soft nature of DPD interaction prevents the system from being caught in a metastable state (what is often observed in the case of the molecular dynamics when atomistic potentials are applied).

We follow the DPD approach as described in Ref. [33]. The length is represented in units of the diameter of the soft bead, and the energy scale is assumed to be $\epsilon^* = k_B T = 1$, where k_B is the Boltzmann constant, T is the temperature and time is expressed in $t^* = 1$. The monomers are connected *via* harmonic springs, which results in a force

$$\mathbf{F}_{ij}^B = -k\mathbf{x}_{ij}, \quad (2)$$

where $\mathbf{x}_{ij} = \mathbf{x}_i - \mathbf{x}_j$ and k is the spring constant. The non-bonded forces contain three

contributions

$$\mathbf{F}_{ij} = \mathbf{F}_{ij}^{\text{C}} + \mathbf{F}_{ij}^{\text{D}} + \mathbf{F}_{ij}^{\text{R}}, \quad (3)$$

where $\mathbf{F}_{ij}^{\text{C}}$ is the conservative force, resulting from the repulsion between i -th and j -th soft beads, $\mathbf{F}_{ij}^{\text{D}}$ is the dissipative force, that occurs due to the friction between soft beads, and random force $\mathbf{F}_{ij}^{\text{R}}$ that works in pair with a dissipative force to thermostat the system. The expressions for all these three contributions are given below [33]

$$\mathbf{F}_{ij}^{\text{C}} = \begin{cases} a(1 - x_{ij}) \frac{\mathbf{x}_{ij}}{x_{ij}}, & x_{ij} < 1, \\ 0, & x_{ij} \geq 1, \end{cases} \quad (4)$$

$$\mathbf{F}_{ij}^{\text{D}} = -\gamma w^{\text{D}}(x_{ij}) (\mathbf{x}_{ij} \cdot \mathbf{v}_{ij}) \frac{\mathbf{x}_{ij}}{x_{ij}^2}, \quad (5)$$

$$\mathbf{F}_{ij}^{\text{R}} = \sigma w^{\text{R}}(x_{ij}) \theta_{ij} \Delta t^{-1/2} \frac{\mathbf{x}_{ij}}{x_{ij}}, \quad (6)$$

where $x_{ij} = |\mathbf{x}_{ij}|$, $\mathbf{v}_{ij} = \mathbf{v}_i - \mathbf{v}_j$, \mathbf{v}_i is the velocity of i th bead, a is the amplitude for the conservative repulsive force. The dissipative force has an amplitude γ and decays with the distance according to the weight function $w^{\text{D}}(x_{ij})$. The amplitude for the random force is σ and the respective weight function is $w^{\text{R}}(x_{ij})$. θ_{ij} is the Gaussian random variable and Δt is the time-step of the simulations. As was shown by Español and Warren [21], to satisfy the detailed balance requirement, the amplitudes and weight functions for the dissipative and random forces should be interrelated: $\sigma^2 = 2\gamma$ and $w^{\text{D}}(x_{ij}) = [w^{\text{R}}(x_{ij})]^2$.

The system is soft repulsive and is kept together by an external pressure to provide the required density, which corresponds to a liquid state. In these simulations the following numeric values are used: $a = 25$ for all pairs of interacting beads, $\gamma = 6.75$, $\sigma = \sqrt{2\gamma} = 3.67$ and the time-step $\Delta t = 0.04$. The duration of all runs (each performed for a different chain length $N = 5 - 40$) was fixed at $8 \cdot 10^6$ DPD steps.

Here and thereafter we consider the case of space dimension $d = 3$ only. All shape characteristics of a chain are derived from the components of the instantaneous gyration tensor \mathbf{Q} defined as in [34, 35]:

$$Q_{\alpha\beta} = \frac{1}{N} \sum_{n=1}^N (x_n^\alpha - X^\alpha)(x_n^\beta - X^\beta) \quad \alpha, \beta = 1, 2, 3. \quad (7)$$

Here, N is the number of monomers of a chain, x_n^α denotes the set of the Cartesian coordinates of n th monomer center: $\mathbf{x}_n = (x_n^1, x_n^2, x_n^3)$, and $X^\alpha = \frac{1}{N} \sum_{n=1}^N x_n^\alpha$ are the coordinates of the center of mass for the chain. Its eigenvectors define the axes of a local frame of a chain and the mass distribution of the latter along each axis is given by the respective eigenvalue λ_i , $i = 1, 2, 3$, respectively. The trace of \mathbf{Q} is an invariant with respect to rotations and is equal to an instantaneous squared gyration radius of the chain

$$R_g^2 = \text{Tr } \mathbf{Q} = 3\bar{\lambda}. \quad (8)$$

Here, the average over three eigenvalues, $\bar{\lambda}$, is introduced to simplify the following expressions.

The instantaneous asphericity A (sometimes also referred to as “the relative shape anisotropy”). The prolateness S and size ratio g are defined as [10, 17, 18, 16]

$$A = \frac{1}{6} \frac{\sum_{i=1}^3 (\lambda_i - \bar{\lambda})^2}{\bar{\lambda}^2}, \quad S = \frac{\prod_{i=1}^3 (\lambda_i - \bar{\lambda})}{\bar{\lambda}^3}, \quad g = \frac{R_e^2}{R_g^2}, \quad (9)$$

where R_e is the magnitude of the end-to-end vector $\mathbf{R}_e = \mathbf{x}_N - \mathbf{x}_1$. A spherical shape is characterised by $A = S = 0$, whereas for a non-spherical one it is: $0 < A < 1$ and $0 < S < 2$ (for prolate shape) and $-1/4 < S < 0$ (for oblate shapes). To define the remaining shape characteristics we follow Ref. [16]. To this end we introduce the following triplet of vectors: \mathbf{r}_1 , \mathbf{r}_2 and \mathbf{r}_3 . Here $\mathbf{r}_1 \equiv \mathbf{R}_e$, \mathbf{r}_2 is the component of the vector $\mathbf{x}_{N/2} - \mathbf{x}_1$ perpendicular to \mathbf{r}_1 , whereas \mathbf{r}_3 is the component of the vector $\mathbf{x}_{N/4} - \mathbf{x}_1$ perpendicular to both \mathbf{r}_1 and \mathbf{r}_2 . For more details, see e.g. Fig. 1 in Ref. [16]. On a technical note, for the case of a non-integer $N/2$ (or $N/4$), the vector $\mathbf{x}_{N/2}$ (or $\mathbf{x}_{N/4}$) was chosen *via* interpolation between the vectors \mathbf{x}_n and \mathbf{x}_{n+1} for the adjacent monomers, where $n = \text{int}(N/2)$ [or $n = \text{int}(N/4)$]. The magnitudes of \mathbf{r}_1 , \mathbf{r}_2 and \mathbf{r}_3 are denoted as r_1 , r_2 and r_3 , respectively. Then, the ratios

$$r_{12} = \frac{r_1}{r_2}, \quad r_{13} = \frac{r_1}{r_3} \quad (10)$$

are evaluated at each time instance.

In real experiments one observes shape characteristics of polymer chains averaged over a sample and over time trajectory. The same can be done in the course of the DPD simulation study. We will denote this hereafter as $\langle \dots \rangle$. Let us note that all expressions [Eqs. (9) – (10)] contain these ratios. Therefore, the averaging can be performed in two ways: as a ratio of the averages or, alternatively, as the average of the ratios, both ways are used in the literature [10, 12, 17, 18, 16]. The former definition leads to the first set of the averages:

$$\hat{A} = \frac{1}{6} \frac{\langle \sum_{i=1}^3 (\lambda_i - \bar{\lambda})^2 \rangle}{\langle \bar{\lambda}^2 \rangle}, \quad \hat{S} = \frac{\langle \prod_{i=1}^3 (\lambda_i - \bar{\lambda}) \rangle}{\langle \bar{\lambda}^3 \rangle}, \quad \hat{g} = \frac{\langle R_e^2 \rangle}{\langle R_g^2 \rangle}, \quad (11)$$

$$\hat{r}_{12} = \frac{\langle r_1 \rangle}{\langle r_2 \rangle}, \quad \hat{r}_{13} = \frac{\langle r_1 \rangle}{\langle r_3 \rangle}, \quad (12)$$

whereas the latter definition yields a second set of averages:

$$\langle A \rangle = \frac{1}{6} \left\langle \frac{\sum_{i=1}^3 (\lambda_i - \bar{\lambda})^2}{\bar{\lambda}^2} \right\rangle, \quad \langle S \rangle = \left\langle \frac{\prod_{i=1}^3 (\lambda_i - \bar{\lambda})}{\bar{\lambda}^3} \right\rangle, \quad \langle g \rangle = \left\langle \frac{R_e^2}{R_g^2} \right\rangle, \quad (13)$$

$$\langle r_{12} \rangle = \left\langle \frac{r_1}{r_2} \right\rangle, \quad \langle r_{13} \rangle = \left\langle \frac{r_1}{r_3} \right\rangle. \quad (14)$$

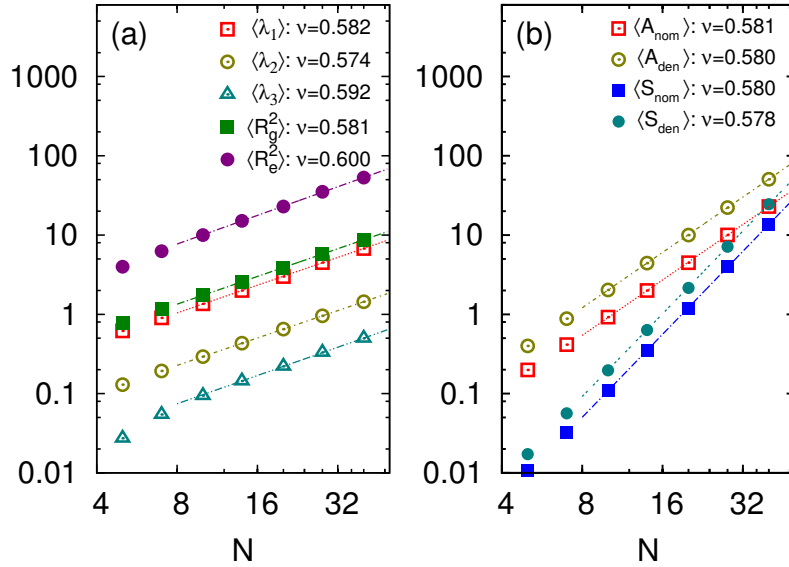


Figure 1. (a) Log-log plot for the average eigenvalues $\langle \lambda_\alpha \rangle$ of the gyration tensor, the squared gyration radius $\langle R_g^2 \rangle$ and the squared end-to-end distance $\langle R_e^2 \rangle$. (b) the same for the average values of asphericity and prolateness nominators and denominators as defined in Eq. (16). N is the number of monomers per chain. Note, that different angles, observed for the two sets of curves in this figure are due to the fact that scaling of A_{nom} and A_{den} is governed by the exponent 4ν , whereas that of S_{nom} and S_{den} – by 6ν , see Eq. (18).

3. Shape characteristic: scaling and the mean values

The scaling laws (1) for the polymer chain in a good solvent modelled by means of the DPD method have previously been discussed in detail [28]. Therefore, we will recall these rather briefly here. In particular, as indicated in Fig. 1 (a), at $N \geq 10$ both $\langle R_g^2 \rangle$ and $\langle R_e^2 \rangle$ obey the expected scaling laws (1) reasonably well yielding an estimate for the Flory exponent falling into the interval of $0.58 < \nu < 0.6$. This is centered around the best known estimate, $\nu = 0.588$, obtained by means of the renormalisation group approach [8].

As far as the asphericity A and the prolateness S of a polymer chain are defined *via* combinations of eigenvalues λ_α of the gyration tensor \mathbf{Q} [see, Eq. 9], the scaling properties of λ_α are also of much interest. Such an analysis for the case of the SAW was performed first in Ref. [36] using lattice MC simulations. It has been demonstrated that the eigenvalues λ_α obey the same scaling laws as the traditional global observables, i.e. R_e and R_g

$$\langle \lambda_\alpha \rangle \sim N^{2\nu}, \quad \alpha = 1, 2, 3, \quad (15)$$

and that the corrections to scaling for the eigenvalues are different but have the same sign as their counterparts for R_g . In our DPD simulations we also find that λ_α obey the same scaling laws as R_g , see, respective legends in Fig. 1 (a). The respective exponents ν for each eigenvalue, obtained *via* linear fit of the data for $N \geq 10$, are indicated in the

same figure and are found to be within the interval $0.574 - 0.592$. This spread of values must be attributed to different magnitudes of the correction to scaling terms [36, 28] in each case. These terms are not accounted for in the current study, as far as accurate values for ν are not the primary goal of this study. Therefore, within the accuracy of our simulations, one may state that the same scaling properties are obeyed by all eigenvalues λ_α of the gyration tensor \mathbf{Q} . This can be interpreted as an isotropicity of the self-similarity properties of a polymer chain.

Due to this statement, and given the definitions for A and S (9), these shape characteristics are expected to be independent of N . To have an additional numerical confirmation for this to hold, we consider the respective nominators and denominators

$$A_{\text{nom}} = \sum_{i=1}^3 (\lambda_i - \bar{\lambda})^2, \quad S_{\text{nom}} = \prod_{i=3}^3 (\lambda_i - \bar{\lambda}), \quad (16)$$

$$A_{\text{den}} = 6\bar{\lambda}^2, \quad S_{\text{den}} = \bar{\lambda}^3, \quad (17)$$

denoted here as “nom” and “den”. Taking into account Eq. (15), one expects the following scaling behaviour

$$\langle A_{\text{nom}} \rangle \sim \langle A_{\text{den}} \rangle \sim N^{4\nu}, \quad \langle S_{\text{nom}} \rangle \sim \langle S_{\text{den}} \rangle \sim N^{6\nu}. \quad (18)$$

The data shown in Fig. 1 (b) indicates that this scaling behaviour holds well for $N \geq 10$ for all four properties defined in Eq. (16) yielding the values of the Flory exponent ν (see the figure) consistent with their counterparts for R_g and λ_α shown in Fig. 1 (a).

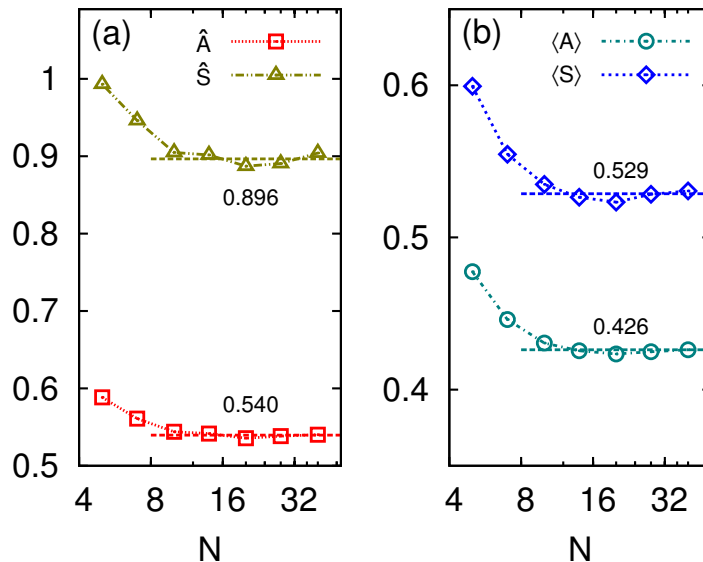


Figure 2. (a) Dependence of the average values \hat{A} and \hat{S} on N . (b) The same for $\langle A \rangle$ and $\langle S \rangle$. Dashed lines indicate the interval of the averaging for evaluating the final mean value.

As a consequence of this, the average values \hat{A} , \hat{S} , $\langle A \rangle$ and $\langle S \rangle$ all demonstrate a weak dependence on N for $N \geq 10$, as shown in Fig. 2. The final mean values for

these characteristics are, therefore, obtained by averaging the data within an interval $10 \leq N \leq 40$, as indicated by dashed lines in both frames of this figure.

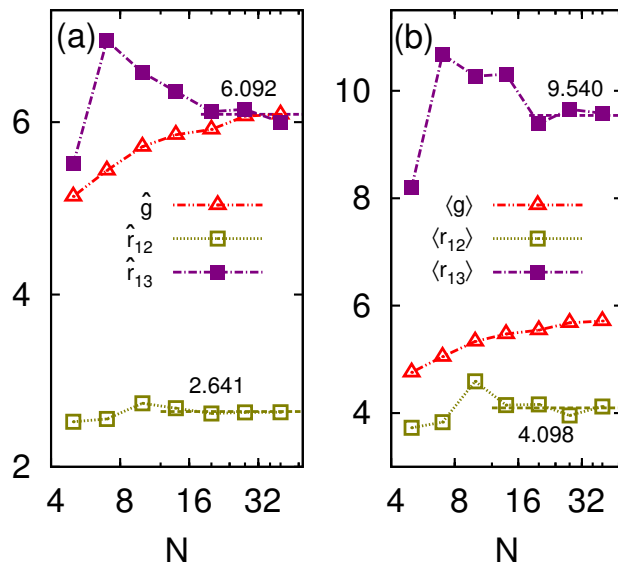


Figure 3. (a) Dependence of the average values \hat{g} , \hat{r}_{12} and \hat{r}_{13} on N . (b) The same for $\langle g \rangle$, $\langle r_{12} \rangle$ and $\langle r_{13} \rangle$. Dashed lines indicate the interval of the averaging for evaluating the final mean value (where applies).

The situation is markedly different for other shape characteristics, where essential N dependence is observed, see Fig. 3. The values for \hat{g} and $\langle g \rangle$ demonstrate steady monotonic growth within the whole interval $5 \leq N \leq 40$ considered in this study. \hat{r}_{13} and $\langle r_{13} \rangle$ stabilize more or less only at $20 \leq N \leq 40$, where the estimate for an average is made. The interval for \hat{r}_{12} and $\langle r_{12} \rangle$ is a slightly broader: $14 \leq N \leq 40$.

The mean values for the shape properties defined in Eqs. (11)-(14) and evaluated in our study as discussed above, are collected in column DPD of Table. 1. Here, we also list the results obtained for SAWs by means of other methods, namely, the direct renormalisation approach [RG (DR)] and Monte Carlo studies (MC), as well as the respective values for the case of random walks (RW). Let us consider \hat{A} and \hat{S} first. One should note that the previous results reported for these characteristics for the case of the SAW, are found to be very close to their counterparts for the RW case. Therefore, a high accuracy is needed to distinguish between both sets unambiguously. In our case of an off-lattice DPD simulations with explicit solvent, this would be very computationally demanding. Nevertheless, within the accuracy limitation of this study, the values found for both \hat{A} and \hat{S} agree reasonably well with the best respective estimates made for the case of SAWs. For the case of $\langle A \rangle$ and $\langle S \rangle$, the difference between the respective values for SAW and RW are more essential. We find reasonably good agreement between our results and other data for SAW in as demonstrated in Fig. 3.

property	SAW				RW
	DPD	RG (DR)	MC	MC ^f	
\hat{A}	0.540	0.529 ^a	0.546 ^c	0.54725	0.526 ^c
\hat{S}	0.896	0.893 ^a		0.91331	0.887 ^a
\hat{g}	> 6	6.258 ^d	6.249 ^b		6 ^a
\hat{r}_{12}	2.641				2.546
\hat{r}_{13}	6.092				5.657
$\langle A \rangle$	0.426	0.415 ^b	0.431 ^b	0.43337	0.394 ^e
$\langle S \rangle$	0.529		0.541 ^b	0.54474	0.475 ^b
$\langle g \rangle$	≤ 6				
$\langle r_{12} \rangle$	4.098				
$\langle r_{13} \rangle$	9.540				
\bar{A}	0.418 [G] 0.390 [L] 0.386 [L']				
\bar{g}	5.333 [G] 5.444 [L]				
\bar{r}_{12}	1.578 [L]				
\bar{r}_{13}	3.763 [L]				

Table 1. The results for mean values of asphericity \hat{A} , $\langle A \rangle$, prolateness \hat{S} , $\langle S \rangle$ and size ratios \hat{g} , $\langle g \rangle$, \hat{r}_{12} , $\langle r_{12} \rangle$, \hat{r}_{13} , $\langle r_{13} \rangle$ defined according to Eqs. (11)-(14) and their respective most probable values \bar{A} , \bar{g} , \bar{r}_{12} and \bar{r}_{13} . The abbreviations stand for: random walk (RW), self avoiding walk (SAW), lattice Monte Carlo (MC), direct renormalization (DR), dissipative particle dynamics (DPD) (this work). Shorthands for citations: ^a [10], ^b [12], ^c [13], ^d [14], ^e [15], ^f [17]. Data obtained *via* fits by Eqs. (21), (22) and (23) are denoted as [G], [L] and [L'], respectively.

4. Shape characteristics probability distributions

It has been observed before [13, 12, 37, 36, 17, 18] that the probability distributions of the shape characteristics of a polymer chain are broad and skewed. This is true for both cases of the RW and SAW and “implies that any description of the shapes of random walks which is based only on mean values of related magnitudes is incomplete” [37]. One of the ways to extend the analysis of the shape characteristics is to complement the mean values by additional characteristic values obtained from the respective probability distributions.

Before we proceed to the probability distributions for the shape characteristics, let us check known asymptotics for the distributions of the end-to-end distance and the gyration radius. To this end we introduce respective reduced properties

$$R_e^* = \frac{R_e}{\langle R_e \rangle}, \quad R_g^* = \frac{R_g}{\langle R_g \rangle}. \quad (19)$$

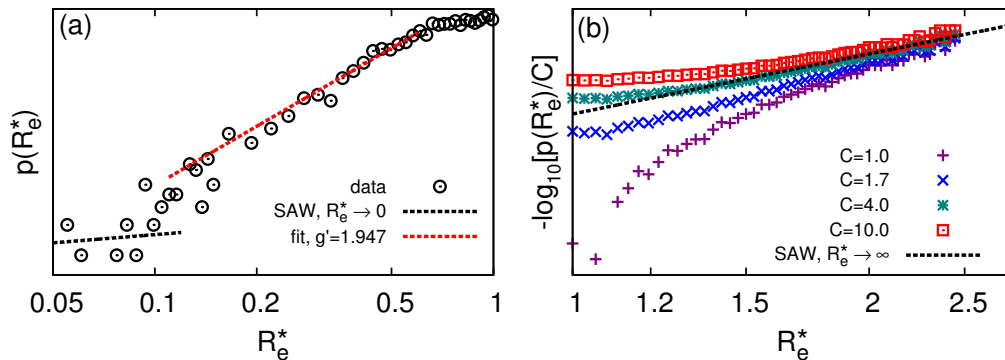


Figure 4. Probability distribution $p(R_e^*)$ for reduced end-to-end distance R_e^* . (a) log-log plot for fitting the asymptotics at $R_e^* \rightarrow 0$. (b) Double log plot for fitting the asymptotics at $R_e^* \gg 0$ built for various trial constant C , see Eq. (20) and the text for more details.

As has been shown in [1, 2], the probability distribution $p(R_e^*)$ has the following asymptotics:

$$p(R_e^*) \approx \begin{cases} A(R_e^*)^{\frac{\gamma-1}{\nu}}, & \text{at } R_e^* \rightarrow 0, \\ C \exp\left[-(R_e^*)^{\frac{1}{1-\nu}}\right], & \text{at } R_e^* \gg 0. \end{cases} \quad (20)$$

where A and C are (non-universal) constants, and $\gamma \approx 1.16$. We built a single cumulative histogram for the probability distribution $p(R_e^*)$ based on simulation data within a scaling regime, i.e. $10 \leq N \leq 40$. To examine its asymptotics at $R_e^* \rightarrow 0$, it was plotted in a log-log scale, see Fig. 4 (a). The $\frac{\gamma-1}{\nu}$ power law is displayed *via* dashed line and is marked as $R_e^* \rightarrow 0$ label. It holds approximately but suffers from somewhat insufficient accuracy near the tail of the distribution (where the statistics is the poorest). However, one also observes a large region of R_e^* values where another power law holds well, namely $(R_e^*)^{g'}$ with $g' \approx 2$. To check for the asymptotics of $p(R_e^*)$ at $R_e^* \gg 0$, the logarithm of the histogram $p(R_e^*)$ is plotted now scaled by the factor C . As this factor is not known *a priori*, we plotted a family of curves using various values for C , see Fig. 4 (b). All curves converge to the exponential asymptotics in Eq. (20), which is shown in the figure *via* a dashed black line. One may conclude therefore that the known asymptotics for the probability distribution $p(R_e^*)$ are adequately reproduced in our simulations.

One should note that the asymptotic regimes (20) are observed rather at extreme values of R_e^* . Therefore, it is of interest whether or not the probability distribution $p(R_e^*)$ can be fitted *via* appropriate analytic expressions reasonably well within a whole interval of R_e^* values. The form for $p(R_e^*)$, as seen in Fig. 5, appears to be weakly asymmetric. Therefore, one of the obvious analytic expressions to apply is a generalised Gaussian one

$$p_G(x) = A \exp\left[-\left(\frac{x-x_0}{\sigma_0}\right)^\delta\right], \quad \bar{x} = x_0. \quad (21)$$

Here and thereafter, the most probable value is denoted as \bar{x} . This fit is marked as [G] in

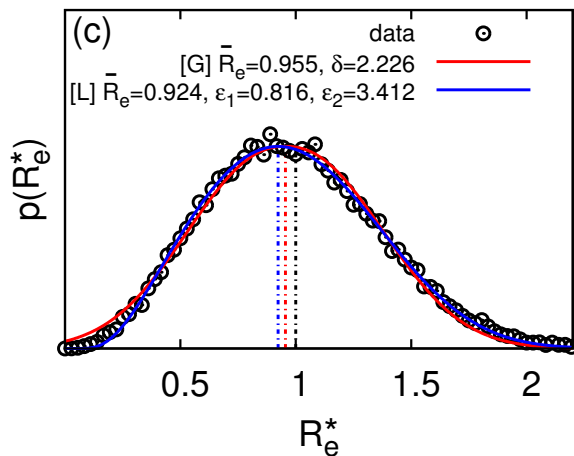


Figure 5. Probability distribution $p(R_e^*)$ and the results of fits according to Eq. (21) (marked as [G]) and Eq. (22) (marked as [L]). The parameters of fits are shown in a figure.

Fig. 5 and yields the exponent $\delta = 2.226$ and the most probable value of $\bar{R}_e = 0.955$. One should remark that this fit closely resembles a standard Gaussian distribution (achieved for parameters values $\delta = 2$ and $\bar{R}_e = 1$). Another choice can be terms of a Lhuillier-like form (for more details, see below)

$$p_L(x) = B \exp \left[- \left(\frac{x'}{x} \right)^{\epsilon_1} - \left(\frac{x}{x'} \right)^{\epsilon_2} \right], \quad \bar{x} = x' \left(\frac{\epsilon_1}{\epsilon_2} \right)^{\frac{1}{\epsilon_1 + \epsilon_2}}. \quad (22)$$

This fit is marked as [L] in Fig. 5 yielding $\epsilon_1 = 0.816$, $\epsilon_2 = 3.412$ and $\bar{R}_e = 0.924$. One may conclude that the values for \bar{R}_e obtained in both fits are very close to the mean value for the scaled end-to-end distance which is equal to one.

Most studies on probability distributions of shape characteristics of polymer chains are undertaken for the case of a Gaussian chain, which mimics the RW [34, 35, 38, 39, 40, 37, 41]. In this case the analytic evaluation is possible, as well as the $1/d$ expansion, all leading to certain analytic expressions for the probability distributions $p(\lambda_\alpha)$ and, in some cases, for $p(A)$ [37, 41]. On the other hand, in most studies that address such probability distributions for the SAW case [12, 17, 18, 16], the authors mainly concentrate on broad shapes of such distributions and compare these with their counterparts for the RW. While an analytic solution for the SAW is not available, there are several indirect options suggesting certain analytic expressions for the probability distributions of interest. One path is suggested by Sciutto [36], where the chi-squared form of the distributions $p(\lambda_\alpha)$ are obtained analytically for the RW is transferred to the SAW case with the different set of parameter values. While the result is very satisfactory for the eigenvalues ratios $\lambda_\alpha/\lambda_\beta$, the probability distributions $p(A)$ and $p(S)$ are not fitted accurately.

Another approach has been suggested by Lhuillier [3], where the empirical form (22) has been deduced for the probability distribution $p(R_g^*)$. In particular, the authors

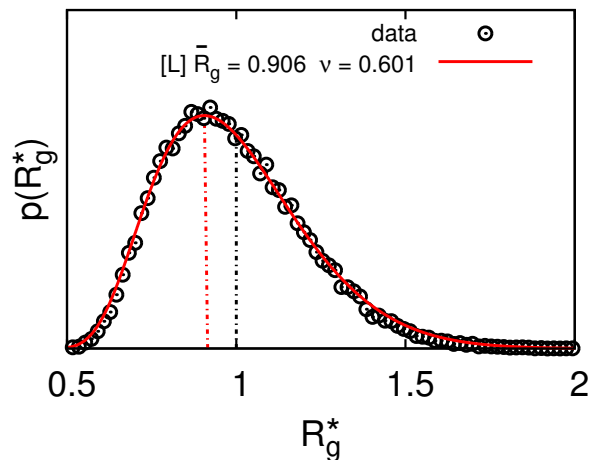


Figure 6. Probability distribution $p(R_g^*)$ and the results of a fit according to Eq. (22) with the exponents $\alpha_1 = \frac{3}{3\nu-1}$ and $\alpha_2 = \frac{1}{1-\nu}$. Most probable value and Flory exponent ν as the result of a fit are shown.

consider statistical weights for extreme cases of collapsed ($R_g^* \rightarrow 0$) and highly stretched ($R_g^* \gg 1$) conformations resulting in the form (22) for the probability distribution $p(R_g^*)$. Both exponents $\alpha_1 = \frac{3}{3\nu-1}$ and $\alpha_2 = \frac{1}{1-\nu}$ are found to depend solely on the Flory exponent ν (for the three-dimensional case). This, therefore, opens up a possibility to have another independent estimate for the exponent ν performing a fit of $p(R_g^*)$ obtained in simulations to the form (22) taking into account the expressions for α_1 and α_2 as functions of ν . Applying this analytic expression (22) to our simulation data we find it to work extremely well, see Fig. 6, yielding the estimate $\nu = 0.601$ for the Flory exponent. It is consistent with previous estimates provided in Figs.1 and 2. The most probable value is $\bar{R}_g = 0.906$ which deviates for about 10% from the mean value equal to one, as the result of an essential asymmetry of the distribution. Due to this asymmetry, the fit used in Eq.(21) makes essentially no sense.

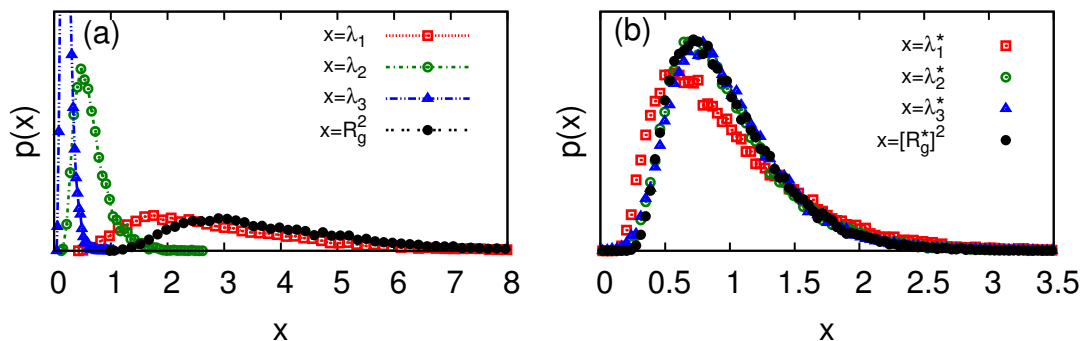


Figure 7. Probability distributions for the eigenvalues λ_α and squared radius of gyration R_g . (a) Distributions for unscaled variables. (b) Distributions for scaled variables, $x^* = x/\langle x \rangle$.

In a further approach, one may consider the probability distributions for the eigenvalues λ_α of the gyration tensor \mathbf{Q} shown in Fig. 7 (a). For the sake of comparison, we also display the probability distribution for their sum, which is equal to R_g^2 . One should note an increase width of the distributions corresponding to an increase of respective eigenvalues $\lambda_1 > \lambda_2 > \lambda_3$. This fact has been already discussed in a number of studies [12, 17, 18, 16]. Another important point whether or not the probability distributions for their scaled counterparts $\lambda_\alpha^* = \lambda_\alpha / \langle \lambda_\alpha \rangle$, $\alpha = 1, 2, 3$ can be mapped onto a single master curve has not discussed so far, except for the case of the RW [34]. There the distributions $p(\lambda_\alpha^*)$ are found not to coincide. Our respective simulation data are displayed in Fig. 7 (b), from which it appears that: (i) the probability distributions $p(\lambda_2^*)$, $p(\lambda_3^*)$ and $p[(R_g^*)^2]$ overlap very closely with little or none deviation, and (ii) while $p(\lambda_1^*)$ does not. Currently, we do not have single physical explanation for point (i) but point (ii) can be explained easily. Let us go back to Fig. 7 (a). In a limit of a highly stretched chain one has $\lambda_2, \lambda_3 \rightarrow 0$ and $R_g^2 \approx \lambda_1 \geq 1$. Hence, at large enough R_g^2 and λ_1 , their respective distributions should overlap. On the other hand, in a most probable, coil state, the contribution to R_g^2 from λ_2 and λ_3 is essentially non-zero. Hence, $R_g^2 > \lambda_1$ and the maximum position for $p(R_g^2)$ is shifted to larger values as compared to that for $p(\lambda_1)$, as observed in Fig. 7 (a). Due to these two requirements, the distributions $p(R_g^2)$ and $p(\lambda_1)$ can not be reduced to the same master curve by the scaling transformation only. We find, however, that the $p(\lambda_1^*)$ distribution can be matched with the others by applying a shift $\lambda_1 \rightarrow \lambda_1 - \langle \lambda_2 + \lambda_3 \rangle$, which is not surprising, as it turns the shifted value into some approximation of the R_g (this is not shown in the figure for a sake of brevity). Nevertheless, one may report relative proximity of the probability distributions for the scaled properties λ_α^* , $\alpha = 1, 2, 3$ and $(R_g^*)^2$ indicating strong isotropicity of the polymer chain along with its eigenvalues. Indeed, not only the mean values for all eigenvalues scale by the same law [Fig. 1 (a)], but also their probability distributions do so to great extent.

The prediction of the asymptotics for the probability distributions of the shape characteristics similar to the way it is done by Lhuillier [3] for R_g faces severe difficulties. Indeed, the interval of small R_g is associated with a collapsed chain, whereas that of large R_g – to highly stretched conformations. This does not hold for the asphericity A , where small (large) values of A contain contributions from the whole range of conformations being spherically symmetric (asymmetric). As was shown in Ref. [36], the form of the probability distributions $p(A)$ and $p(S)$ differ for the cases of SAW and RW. Therefore, reparametrisation of the chi-squared expressions valid for a RW do not reproduce well the respective distributions for the SAW case. In this paper we chose another route: reparametrisation of the Lhuillier-like expression (22), heuristically suggested for the gyration radius distribution, and its extension for the distribution of shape characteristics.

Similarly to the cases of the R_e and R_g probability distributions, we build a cumulative probability distribution histogram for each shape characteristic based on the simulation data for $N = 10, 14, 20, 28$ and 40 . As was shown in Figs. 1-3, within this

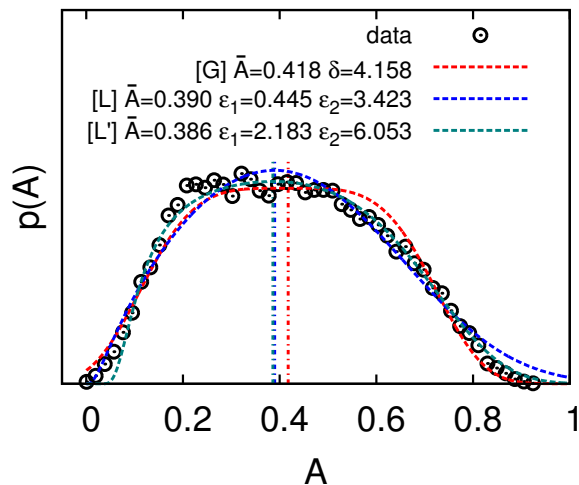


Figure 8. Probability distribution $p(A)$ and the results of fits according to Eq. (21) (marked as [G]), Eq. (22) (marked as [L]) and Eq. (23) (marked as [L']). The parameters of fits are shown in a figure.

interval of N the scaling laws follow sufficiently well and the probability distributions are found to overlap. The study of such a cumulative histogram essentially enhances the statistics of the analysed data.

The form of the probability distribution $p(A)$ for the asphericity, shown in Fig. 8, indicates a relatively low asymmetry, therefore we attempt fits using both functional forms (21) and (22). This yield the following exponents: $\delta = 4.158$, $\epsilon_1 = 0.445$ and $\epsilon_2 = 3.423$ and the most probable values $\bar{A} = 0.418$ and 0.390 for $p_G(A)$ and $p_L(A)$, respectively. The fit *via* Lhuillier-like form follows the shape of $p(A)$ more closely. An even better approximation can be achieved by using the extended Lhuillier-like form

$$p'_L(x) = C \exp \left[- \left(\frac{x_1}{x} \right)^{\epsilon_1} - \left(\frac{x}{x_2} \right)^{\epsilon_2} \right], \quad \bar{x} = \left(x_1^{\epsilon_1} x_2^{\epsilon_2} \frac{\epsilon_1}{\epsilon_2} \right)^{\frac{1}{\epsilon_1 + \epsilon_2}}. \quad (23)$$

In this case the exponents are: $\epsilon_1 = 2.183$ and $\epsilon_2 = 6.053$ and the most probable value for the asphericity is $\bar{A} = 0.386$. This is very close to the one obtained with the (22) form. The most probable values \bar{A} are added to Tab. 1 and one notes that the value obtained from the fit (21) is close to the average value $\langle A \rangle$, whereas both values obtained *via* fits (22) and (23) are closer to the asphericity of a RW.

The prolateness S , as already mentioned above, distinguishes between the oblate ($S < 0$) and prolate ($S > 0$) conformations of a chain. The shape of its probability distribution, $p(S)$, is also markedly different in these two intervals of S values, see Fig. 9. We were unable to fit it by a single analytic form but instead opted for two separate fits, at $S < 0$ and $S > 0$

$$p(S) = \begin{cases} A(S + 0.25)^\beta, & S < 0, \\ B \exp \left[- \left(\frac{x}{x_0} \right)^{\epsilon_2} \right], & S > 0. \end{cases} \quad (24)$$

The analytic form used for $S > 0$ can be attributed to a limit case of both Eq. (21) (at

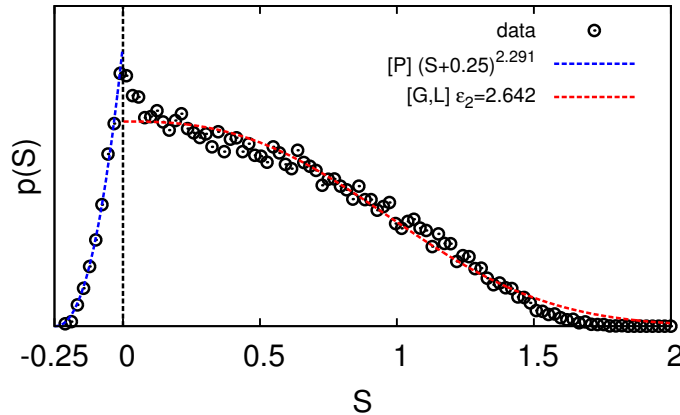


Figure 9. Probability distribution $p(S)$ and the results of a fit according to Eq. (24). The parameters of a fit are shown in a figure.

$x_0 = 0$) and of Eq. (23) (at $x_1 = 0$), therefore this fit is marked as [G, L' or L] in Fig. 9. One can not define the most probable value \bar{S} for the prolateness from a fit (24).

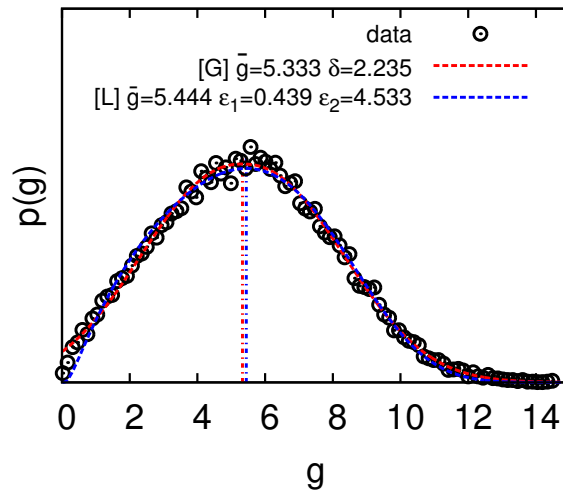


Figure 10. Probability distribution $p(g)$ and the results of fits according to Eq. (21) (marked as [G]) and Eq. (22) (marked as [L]). The parameters of fits are shown in the figure.

The probability distribution $p(g)$ for the size ratio g is shown in Fig. 10. It is fitted similarly to the $p(A)$ distribution, *via* analytic forms (21) and (22). This yields the respective exponents $\delta = 2.235$, $\epsilon_1 = 0.439$ and $\epsilon_2 = 4.533$. The most probable values are $\bar{g} = 5.333$ and 5.444 , respectively. One should note that other approaches evaluate the \hat{g} value only which is equal to 6 for the RW and is found to be larger than 6 for the SAW (see, Tab. 1). It is evident from Fig. 3 that reliable estimates for both \hat{g} and $\langle g \rangle$ require the use of a polymer chain longer than $N = 40$ (maximal length used in this study) and, therefore, can not be provided within this study. Therefore, the most probable values \bar{g} obtained here do not have any counterparts to be compared with and

can serve as an indication of high asymmetry of the $p(g)$ distribution only.

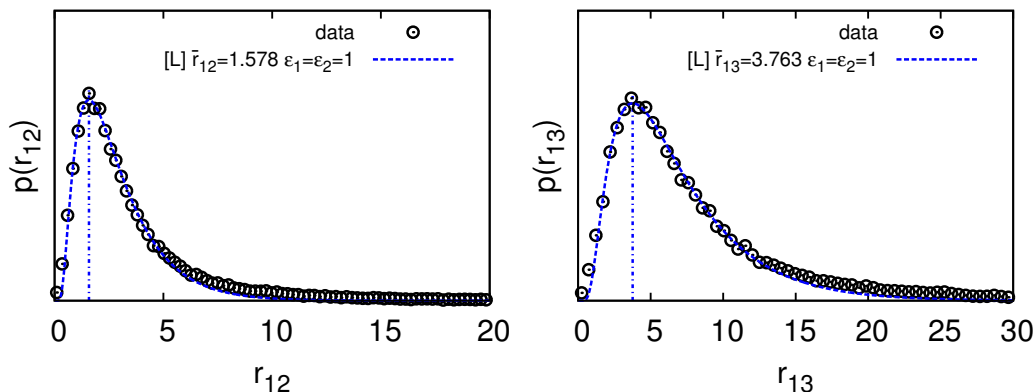


Figure 11. (a) Probability distribution $p(r_{12})$ and the results of a fit according to Eq. (22) with fixed $\epsilon_1 = \epsilon_2 = 1$ (marked as [L]). (b) The same for $p(r_{13})$. The parameters of fits are shown in the figure.

The probability distributions $p(r_{12})$ and $p(r_{13})$ appear to be of a similar, highly asymmetric form, see Fig. 11 (a) and (b). Both were preliminarily fitted by the general expression (22) yielding the exponents ϵ_1 and ϵ_2 close to 1. Therefore, in the final fits we set $\epsilon_1 = \epsilon_2 = 1$ and obtain the following estimates for the most probable values: $\bar{r}_{12} = 1.578$ and $\bar{r}_{13} = 3.763$, the fits are shown in Fig. 11. These values differ about 2.5–3 times from their counterparts $\langle r_{12} \rangle$ and $\langle r_{13} \rangle$ (see, Tab. 1) due to high asymmetry of respective distributions.

5. Conclusions

Here we have analysed the shape characteristics of a coarse-grained polymer chain in a good solvent using DPD simulations. One of the aims was to check the universality of the properties not directly connected to the scaling power laws. In this respect we here evaluated the shape characteristics which can be seen as counterparts of the universal critical amplitude ratios in critical phenomena.

As far as the simulations employ an off-lattice model for the polymer chain and an explicit solvent, these are more computationally intensive than their lattice Monte Carlo counterparts and can not match the latter in numerical accuracy. However, using this simulation technique, one bridges the gap to a large number of studies targeted on at self-assembly of various amphi- and polyphilic systems and to the flow-driven phenomena on the nanoscale. Hence, according to our aim, we rather focus on a qualitative analysis of the mean and most probable values for the shape characteristics, as well as on the form of their probability distributions. Therefore, no rigorous analysis of the numerical errors was performed and these are not displayed in the figures or in the table of results.

The origin our analysis is a study of the scaling properties of the gyration tensor components. We find that, for chain lengths $N \geq 10$, not only the end-to-end distance

and gyration radius, but also all three eigenvalues of the gyration tensor scale with the same power law. The Flory exponent ν obtained for each of these properties independently, within the accuracy of the simulations, is close to the best theoretical estimate $\nu = 0.588$. Based on the analytic expressions, the shape characteristics of the chain are expected to be independent of N in the same interval of chain lengths. This has been checked by plotting each of them against N .

The mean values for the shape characteristics were evaluated by averaging their respective values obtained for chain lengths of $N = 10, 14, 20, 28$ and 40 . The mean values for the asphericity and prolateness are found to compare well with the respective results obtained by means of other approaches, whereas the shape anisotropy requires simulations of longer chains. The averaging procedure for these properties, however, is found to be rather ambiguous, as the probability distributions for all shape characteristics are wide and many are highly asymmetric. Therefore, alongside with the mean values, one may consider looking at the most probable values of each characteristic as well. This can be performed by fitting the probability distribution for each characteristic by certain analytic expressions and determining the most probable value based on the positions of its maxima.

Here, we started from the analysis of the probability distributions for the reduced end-to-end distance and the gyration radius. For the former case, the known analytic asymptotics of Cloiseaux-de Gennes were reproduced, whereas for the latter the Lhuillier analytic expression is found to be very accurate yielding another independent estimate for the Flory exponent ν . The analytic expressions in both cases are based on an analysis of the conformation statistics, which is more difficult to apply to the shape characteristics. For the latter, we suggest heuristic analytic expressions based on the Lhuillier form and, for the symmetric distributions, on a generalised Gaussian distribution. This leads to simple analytical expressions with the coefficients and exponents found from fitting the simulation data. This allows us to complement the mean values for the shape properties by their most probable values found as the maximal positions of the respective distributions.

The study can be interpreted as yet another validation on the appropriateness of the use of soft coarse-grained potentials to describe the self-avoiding polymer chain. Not only the scaling properties of the end-to-end distance and gyration radius of such chains are in good agreement with the theoretical data, but also the mean values of the shape characteristics and their probability distributions are found to closely mimic the results of more accurate lattice Monte Carlo simulations.

Acknowledgements

We are thankful to Victoria Blavatska for useful discussions. This work was supported in part by FP7 EU IRSES projects No. 295302 “Statistical Physics in Diverse Realizations”, No. 612707 “Dynamics of and in Complex Systems”, No. 612669 “Structure and Evolution of Complex Systems with Applications in Physics and Life

Sciences”, and by the Doctoral College for the Statistical Physics of Complex Systems, Leipzig-Lorraine-Lviv-Coventry (\mathbf{L}^4).

- [1] de Gennes P G 1979 *Scaling Concepts in Polymer Physics* (Cornell University Press Ithaca London)
URL <http://dx.doi.org/10.1063/1.2914118>
- [2] des Cloizeaux J 1982 Theory of polymers in solution *Phase Transitions Cargèse 1980* (Springer Science + Business Media) pp 371–394 URL
http://dx.doi.org/10.1007/978-1-4613-3347-0_16
- [3] Lhuillier D 1988 *J. Phys. France* **49** 705–710 URL <http://dx.doi.org/10.1051/jphys:01988004905070500>
- [4] Arunchander A, Peera S G, Parthiban V, Akula S, Kottakkat T, Bhat S D and Sahu A K 2015
RSC Adv. **5** 75218–75228 URL <http://dx.doi.org/10.1039/C5RA15233J>
- [5] Anderson W C, Rhinehart J L, Tennyson A G and Long B K 2016 *J. Am. Chem. Soc.* **138** 774–777
URL <http://dx.doi.org/10.1021/jacs.5b12322>
- [6] Striegel A M, Yau W W, Kirkland J J and Bly D D 2009 *Modern Size-Exclusion Liquid Chromatography* (Wiley-Blackwell) URL <http://dx.doi.org/10.1002/9780470442876>
- [7] Kuhn W 1936 *Angewandte Chemie* **49** 858–862 URL <http://dx.doi.org/10.1002/ange.19360494803>
- [8] Guida R and Zinn-Justin J 1998 *J. Phys. A: Math. Gen.* **31** 8103–8121 URL
<http://dx.doi.org/10.1088/0305-4470/31/40/006>
- [9] Zinn-Justin J 2002 *Quantum Field Theory and Critical Phenomena* (Oxford University Press (OUP)) URL <http://dx.doi.org/10.1093/acprof:oso/9780198509233.001.0001>
- [10] Aronovitz J and Nelson D 1986 *J. Phys. France* **47** 1445–1456 URL
<http://dx.doi.org/10.1051/jphys:019860047090144500>
- [11] Cannon J W, Aronovitz J A and Goldbart P 1991 *J. Phys. I France* **1** 629–645 URL
<http://dx.doi.org/10.1051/jp1:1991159>
- [12] Jagodzinski O, Eisenriegler E and Kremer K 1992 *J. Phys. I France* **2** 2243–2279 URL
<http://dx.doi.org/10.1051/jp1:1992279>
- [13] Bishop M and Saltiel C J 1988 *The Journal of Chemical Physics* **88** 6594 URL
<http://dx.doi.org/10.1063/1.454446>
- [14] Benhamou M and Mahoux G 1985 *Journal de Physique Lettres* **46** 689–693 URL
<http://dx.doi.org/10.1051/jphyslet:019850046015068900>
- [15] Diehl H W and Eisenriegler E 1989 *J. Phys. A: Math. Gen.* **22** L87–L91 URL
<http://dx.doi.org/10.1088/0305-4470/22/3/005>
- [16] Blavatska V, von Ferber C and Holovatch Y 2011 *Condensed Matter Physics* **14** 33701 URL
<http://dx.doi.org/10.5488/CMP.14.33701>
- [17] Zifferer G 1999 *The Journal of Chemical Physics* **110** 4668–4677 URL
<http://dx.doi.org/10.1063/1.478350>
- [18] Zifferer G 1999 *Macromolecular Theory and Simulations* **8** 433–462 URL
[http://dx.doi.org/10.1002/\(SICI\)1521-3919\(19990901\)8:5<433::AID-MATS433>3.0.CO;2-C](http://dx.doi.org/10.1002/(SICI)1521-3919(19990901)8:5<433::AID-MATS433>3.0.CO;2-C)
- [19] Victor J M and Lhuillier D 1990 *The Journal of Chemical Physics* **92** 1362–1364 URL
<http://dx.doi.org/10.1063/1.458147>
- [20] Hoogerbrugge P J and Koelman J M V A 1992 *Europhysics Letters (EPL)* **19** 155–160 URL
<http://dx.doi.org/10.1209/0295-5075/19/3/001>
- [21] Español P and Warren P 1995 *Europhysics Letters (EPL)* **30** 191–196 URL
<http://dx.doi.org/10.1209/0295-5075/30/4/001>
- [22] Schlijper A G 1995 *Journal of Rheology* **39** 567 URL <http://dx.doi.org/10.1122/1.550713>
- [23] Kong Y, Manke C W, Madden W G and Schlijper A G 1997 *The Journal of Chemical Physics*
107 592 URL <http://dx.doi.org/10.1063/1.474420>
- [24] Spenley N A 2000 *Europhysics Letters (EPL)* **49** 534–540 URL
<http://dx.doi.org/10.1209/epl/i2000-00183-2>
- [25] Symeonidis V, Karniadakis G E and Caswell B 2005 *Phys. Rev. Lett.* **95** URL
<http://dx.doi.org/10.1103/PhysRevLett.95.076001>
- [26] Jiang W, Huang J, Wang Y and Laradji M 2007 *The Journal of Chemical Physics* **126** 044901
URL <http://dx.doi.org/10.1063/1.2428307>
- [27] Nardai M M and Zifferer G 2009 *The Journal of Chemical Physics* **131** 124903 URL

- <http://dx.doi.org/10.1063/1.3231854>
- [28] Ilnytskyi J M and Holovatch Y 2007 *Condensed Matter Physics* **10** 539 URL <http://dx.doi.org/10.5488/CMP.10.4.539>
- [29] Ilnytskyi J M, Patsahan T, Holovko M, Krouskop P E and Makowski M P 2008 *Macromolecules* **41** 9904–9913 URL <http://dx.doi.org/10.1021/ma801045z>
- [30] Ilnytskyi J M, Patsahan T and Sokolowski S 2011 *The Journal of Chemical Physics* **134** 204903 URL <http://dx.doi.org/10.1063/1.3592562>
- [31] Ilnytskyi J M, Sokolowski S and Patsahan T 2013 *Condensed Matter Physics* **16** 13606 URL <http://dx.doi.org/10.5488/CMP.16.13606>
- [32] Ilnytskyi J M, Bryk P and Patrykiewicz A 2016 *Condensed Matter Physics* **19** 13609 URL <http://dx.doi.org/10.5488/CMP.19.13609>
- [33] Groot R D and Warren P B 1997 *The Journal of Chemical Physics* **107** 4423 URL <http://dx.doi.org/10.1063/1.474784>
- [34] Šolc K 1971 *The Journal of Chemical Physics* **54** 2756 URL <http://dx.doi.org/10.1063/1.1675241>
- [35] Šolc K and Stockmayer W H 1971 *The Journal of Chemical Physics* **55** 335 URL <http://dx.doi.org/10.1063/1.1675527>
- [36] Sciutto S J 1996 *J. Phys. A: Math. Gen.* **29** 5455–5473 URL <http://dx.doi.org/10.1088/0305-4470/29/17/019>
- [37] Sciutto S J 1994 *J. Phys. A: Math. Gen.* **27** 7015–7034 URL <http://dx.doi.org/10.1088/0305-4470/27/21/017>
- [38] Rudnick J and Gaspari G 1986 *J. Phys. A: Math. Gen.* **19** L191–L193 URL <http://dx.doi.org/10.1088/0305-4470/19/4/004>
- [39] Gaspari G, Rudnick J and Beldjenna A 1987 *J. Phys. A: Math. Gen.* **20** 3393–3414 URL <http://dx.doi.org/10.1088/0305-4470/20/11/041>
- [40] Wei G and Eichinger B E 1990 *Macromolecules* **23** 4845–4855 URL <http://dx.doi.org/10.1021/ma00224a013>
- [41] Sciutto S J 1995 *J. Phys. A: Math. Gen.* **28** 3667–3679 URL <http://dx.doi.org/10.1088/0305-4470/28/13/012>